Supporting Information for:

Role of Lead Vacancies for Optoelectronic Properties of Lead-Halide Perovskites

Dayton J. Vogel,[a] Talgat M. Inerbaev,[b,c] Dmitri S. Kilin[a,d]

[a]Department of Chemistry, University of South Dakota, Vermillion, SD 57069

[b]L.N. Gumilyov Eurasian National University, Astana 010008, Kazakhstan

[c]National University of Science and Technology MISIS, Moscow, 119049 Russian Federation

[d]Department of Chemistry and Biochemistry, North Dakota State University, Fargo, ND, 58108

Corresponding author: Dmitri.Kilin@ndsu.edu

The manuscript reports consequences of creating a Pb vacancy in the bulk perovskite material leading to an additional unoccupied electronic state that provides (a) additional structural rearrangements, such as I_2 formation and (b) new pathways for relaxation of a photo excitation. Anionic open-shell configuration made by addition of an extra electron into the Pb vacancy localizes the frontier orbitals around the Pb vacancy thus affecting relaxation mechanism. The relaxation pathways for spin majority and spin minority components exhibit drastically different contributions to energy relaxation and to photoemission. This observation can be applied to increase control and tune-ability of materials for optoelectronic and photovoltaic applications.

Non-collinear spin DFT as implemented in VASP has been used to calculate the effects of spin orbit coupling upon the ground state electronic structure of the modeled systems.[1-3] This methodology has been detailed in previous work.[4] The relativistic Hamiltonian, $H^{\text{relativistic}} = H^{SR} + H^{SOC}$, is used where H^{SR} and H^{SOC} correspond to scalar relativistic and spin-orbit terms, respectively. The second-order approximation of SOC term is $H^{SOC} = \frac{\hbar}{4m^2c^2}\frac{1}{r}\frac{\partial v^{KS}_{\text{sphere}}}{\partial r}\vec{L}\cdot\vec{S}$ where v^{KS}_{sphere} is given by the spherical harmonics, $\vec{L}$ is the angular momentum operator, and $\vec{S}$ is Pauli spin matrices. Results of SOC calculations in the basis of KSO are presented as components of spinor orbitals $\sum_{\sigma=\alpha,\beta}\left(-\delta_{\sigma\sigma'}\nabla^2 + v^{eff}_{\sigma\sigma'}(\vec{r})\right)\varphi_{i\sigma}(\vec{r}) = \varepsilon_i^{NCS}\,\varphi_{i\sigma'}(\vec{r})$. The spinor KSO is a two-component vector, $\varphi_i^{KS}(\vec{r}) = \begin{Bmatrix}\varphi_{i\alpha}(\vec{r})\\ \varphi_{i\beta}(\vec{r})\end{Bmatrix}, |\varphi_{i\alpha}|^2 + \left|\varphi_{i\beta}\right|^2 = 1$. Using the spinor form the transition dipole moment can be found using $\langle\vec{D}_{ij}\rangle = \int\{\varphi^*_{i\alpha} \quad \varphi^*_{i\beta}\}\vec{r}\begin{Bmatrix}\varphi_{j\alpha}\\ \varphi_{j\beta}\end{Bmatrix}\vec{r} = \int d\vec{r}\left(\varphi^*_{i\alpha}(\vec{r})\,\vec{r}\varphi_{j\alpha}(\vec{r}) + \varphi^*_{i\beta}(\vec{r})\vec{r}\,\varphi_{j\beta}(\vec{r})\right)$. The SOC transition dipole moment is then used to produce absorption spectra through the methods described in the methodology.

The transition dipole moment matrix elements, $\vec{D}_{ij}$, can be constructed $\vec{D}_{ij} = \langle i|\hat{D}|j\rangle = \sum_{G,G'<G_{cut}} C^*_{i,G}D_{G,G'}C_{j,G'}$ with the matrix element, $D_{G,G'}$, defined as $D_{G,G'} = -e\int d^3r e^{iGr}re^{-iG'r}$. The dipole matrix elements are re-expressed in terms of momentum operator matrix elements, $\langle i|\hat{p}|j\rangle = i\hbar\sum_{G,G'<G_{cut}} C^*_{i,G}D_{G,G'}C_{j,G'}$ to obtain $\langle i|\hat{D}|j\rangle = \langle i|\hat{p}|j\rangle\frac{i\hbar e}{m_e(\varepsilon_j-\varepsilon_i)}$.

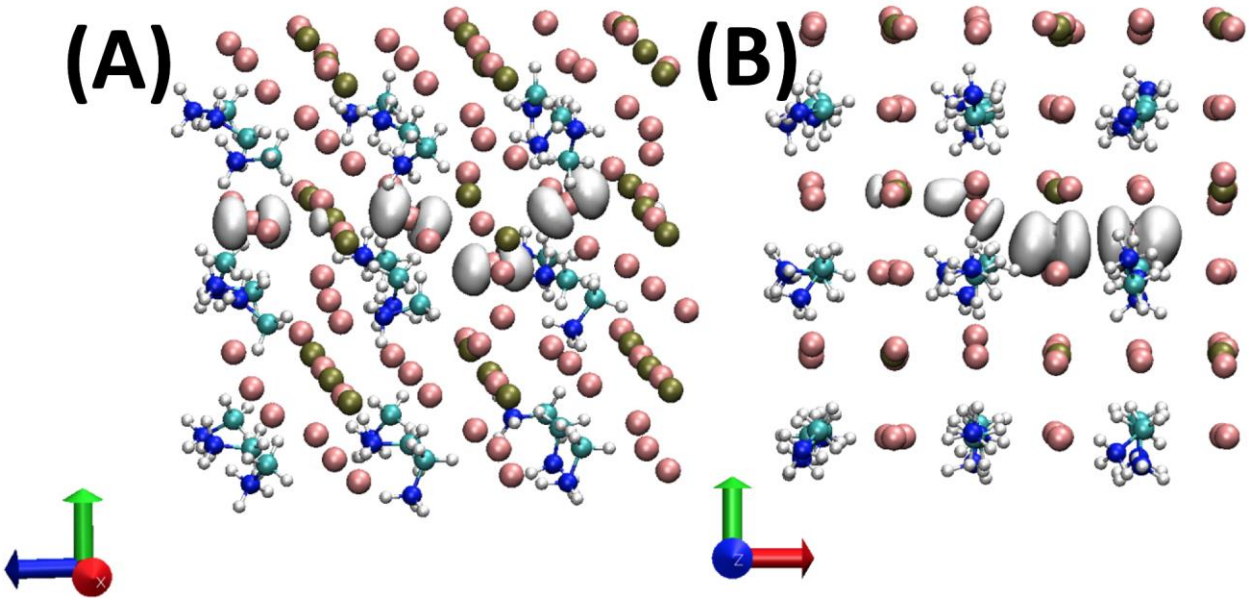

Figure S1. Partial charge density of the ground state optimized HOMO (A) and LUMO (B) states for the V_{Pb} neutral model.

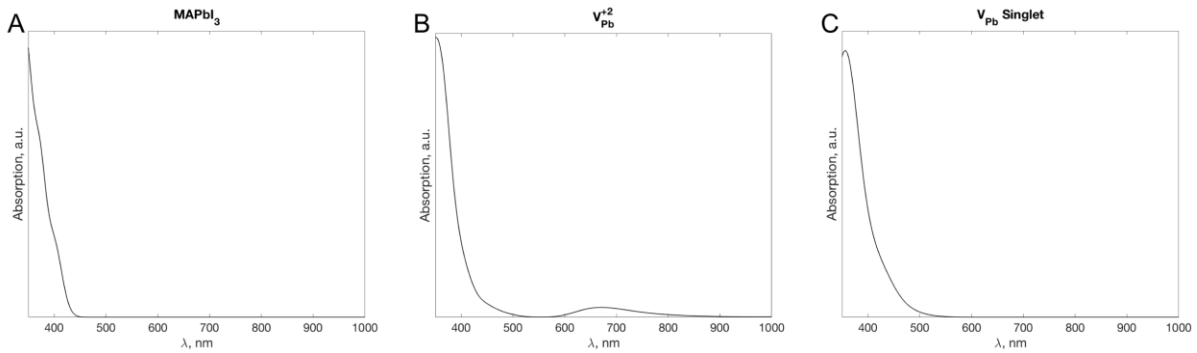

Figure S2. Absorption spectra calculated for the ground state electronic structure of the (A) $MAPbI_3$, (B) V_{Pb}^{+2}, and (C) $V_{Pb,S=0}$. Addition of a Pb vacancy in **panel B** shows the introduced red shifted peak due to the formation of an unoccupied state within the band gap. Charge correction in **panel C** shows a slight red shift to the absorption onset.

Comparison of calculated band dispersion for the $MAPbI_3$, V_{Pb}^{+2}, and $V_{Pb,S=0}$ models highlight new states introduced due to vacancy creation, as shown in **Fig. S3.** As predicted, the vacancy state within the band gap is shown to be relatively consistent across high symmetry points sampled, $\varepsilon_i(\vec{k}) \approx const$.

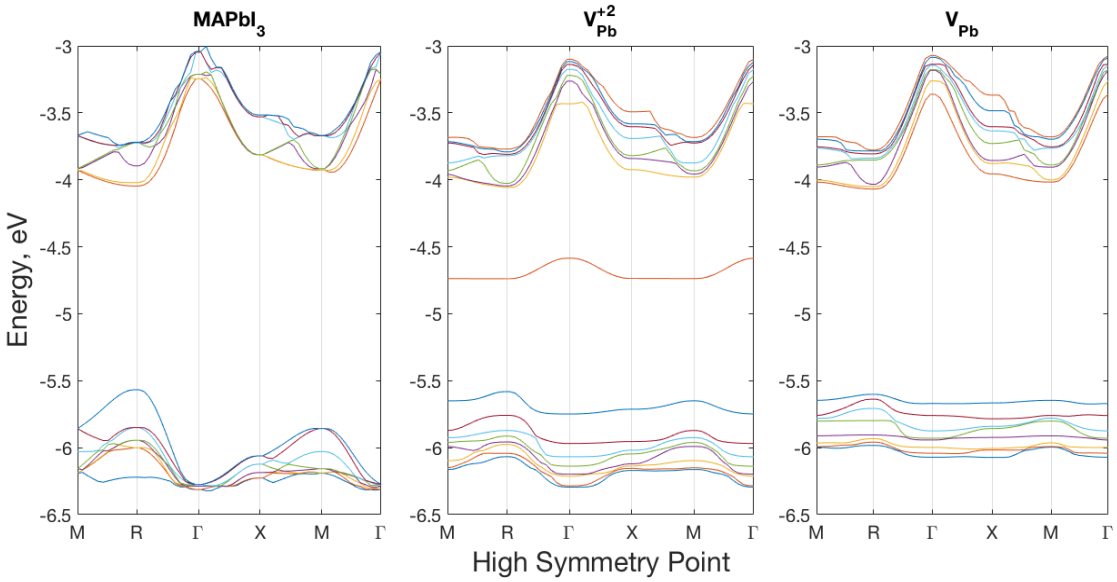

Figure S3. Band structure calculations performed for the three closed shell systems. The vacancy state created in the V_{Pb}^{+2} system shows a sustained defect band across multiple k-points with a small change in energy.

To compare the effects of unit cells within a simulation cell and the resulting location of direct band gap location a smaller, 2x2x2 super cell, was used to calculate the band structure. Below in **Fig. S4** with a reduced super cell the band gap is pushed back to the gamma point.

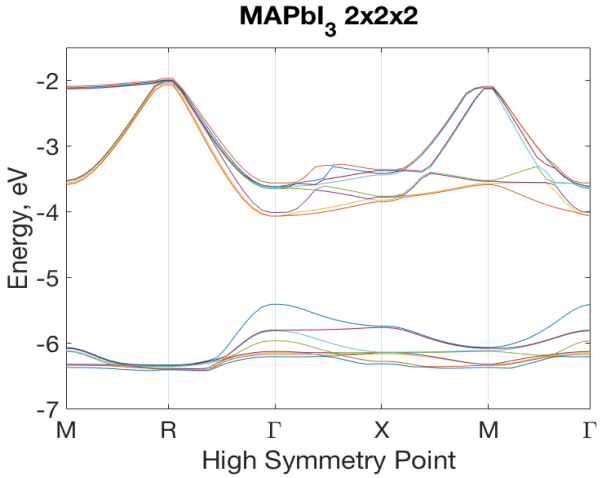

Figure S4. Band structure calculated for a 2x2x2 super cell composed of cubic $MAPbI_3$ unit cells. The choice of super cell size can direct the high symmetry point at which the direct band gap is located.

The models under study are sensitive to the geometry of the material. Absorption spectra for larger super cells, 4x4x4 and 5x5x5, show geometry induced folding of the band structure to the gamma point for even numbered super cells. It is also important to note the effect of including all k-points of the system. By removing possible electronic transitions away from the gamma point, the intensity and features of the absorption spectra (left panel) are greatly modified.

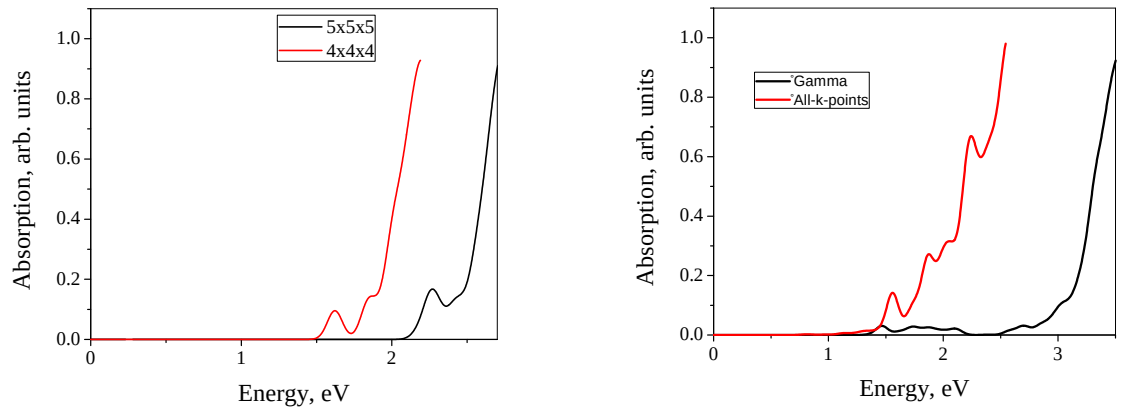

Figure S5. Absorption spectra for a 4x4x4 and 5x5x5 super cell, left panel. Absorption spectra for V_{Pb}^{+2} model at gamma and including all k-points of a 2x2x2 mesh.

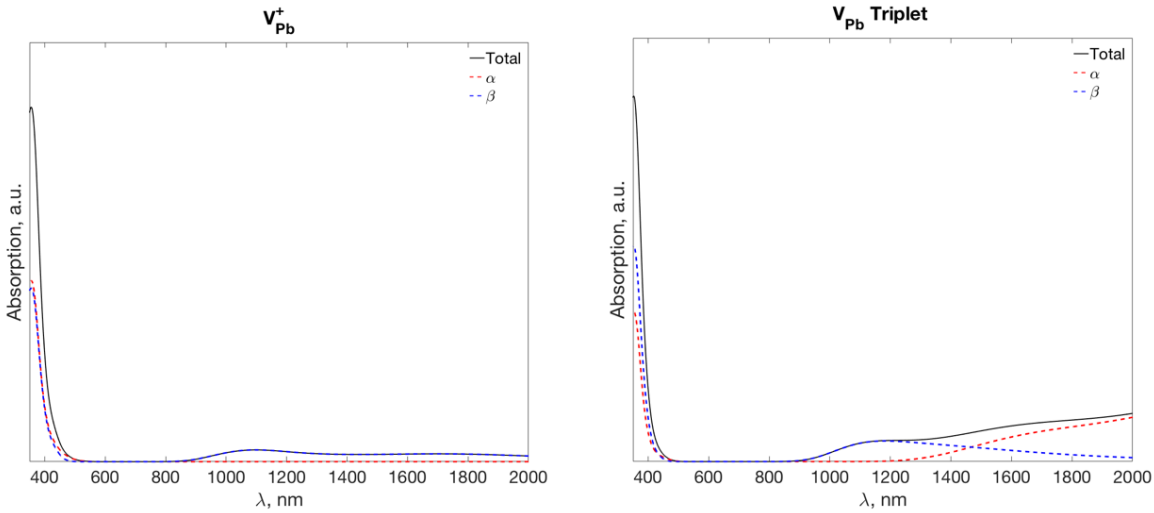

Figure S6. Absorption spectra for both open shell structures providing total absorption contributions from both α and β spin projections. The solid (black), red (dashed), and blue (dashed) lines represent the total, α, and β spectra, respectively.

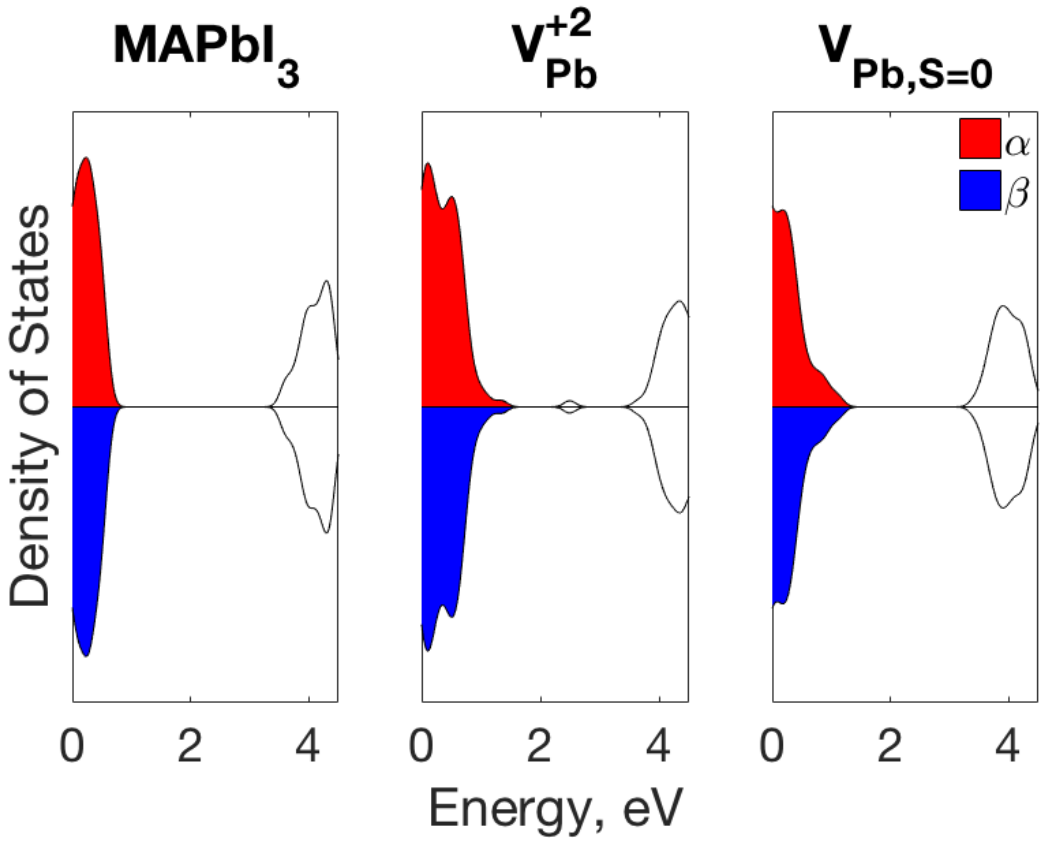

Figure S7. Spin polarized DOS for closed shell electronic configurations. The symmetric DOS for both up and down spin projections highlight the fact that they have all electrons paired in the ground state.

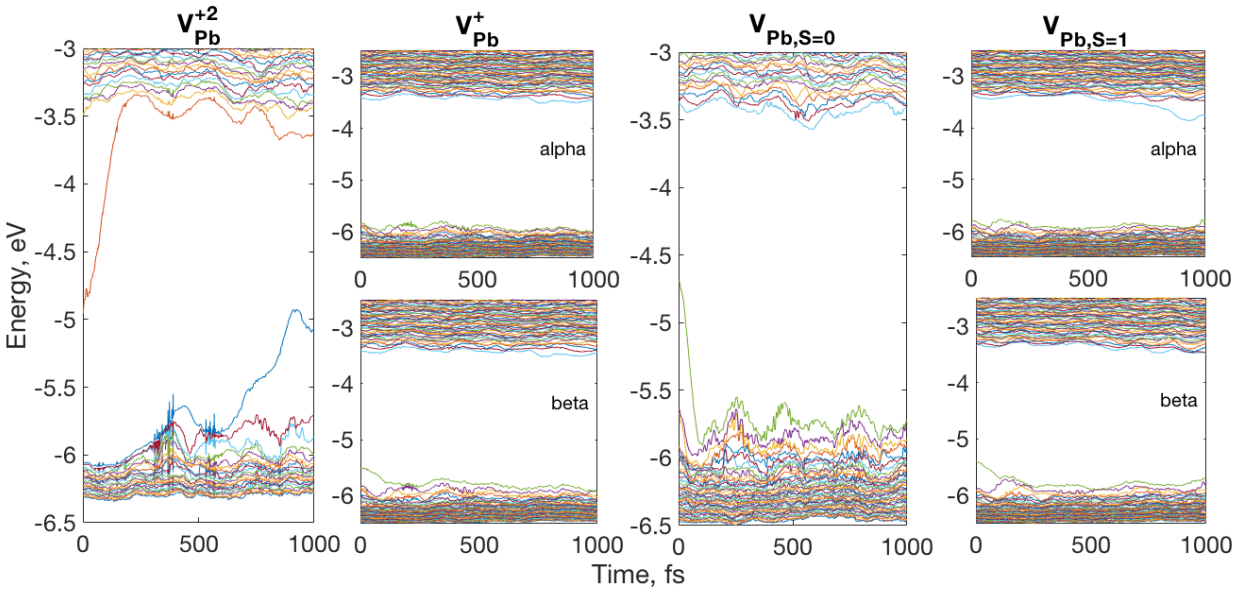

Figure S8. Kohn-Sham orbital energy fluctuations along the ground state molecular dynamic trajectory for all Pb vacancy models. During the V_{Pb}^{+2} dynamic trajectory, the dopant state created by the Pb vacancy migrates from the middle of the band gap to the bottom of the conduction band. The migrating dopant energy corresponds to the production of an I_2 molecule at the Pb vacancy site.

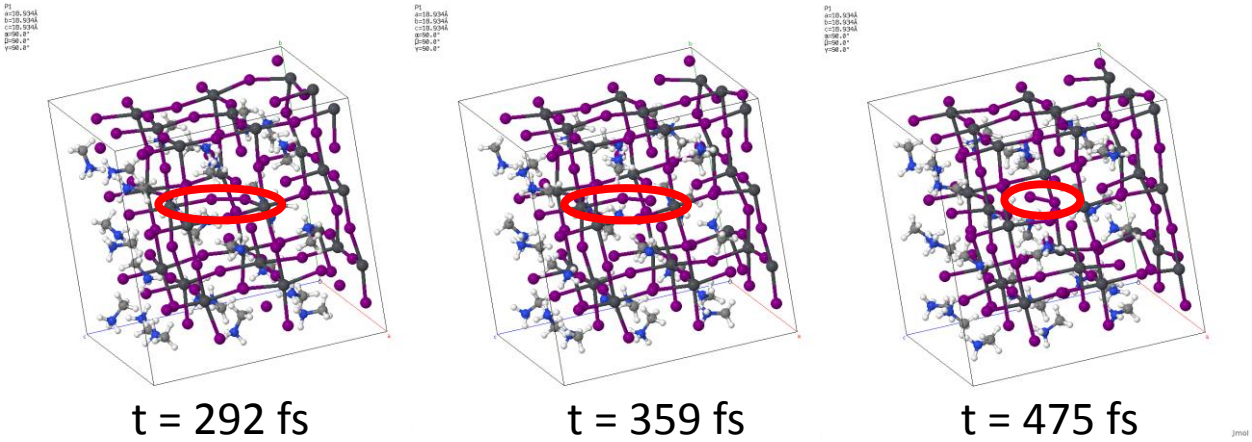

Figure S9. Three snapshots along the V_{Pb} molecular dynamic trajectory show the evolution of a free formed I_2 molecule at the Pb defect site. The I_2 molecule is circled in red to highlight the formation.

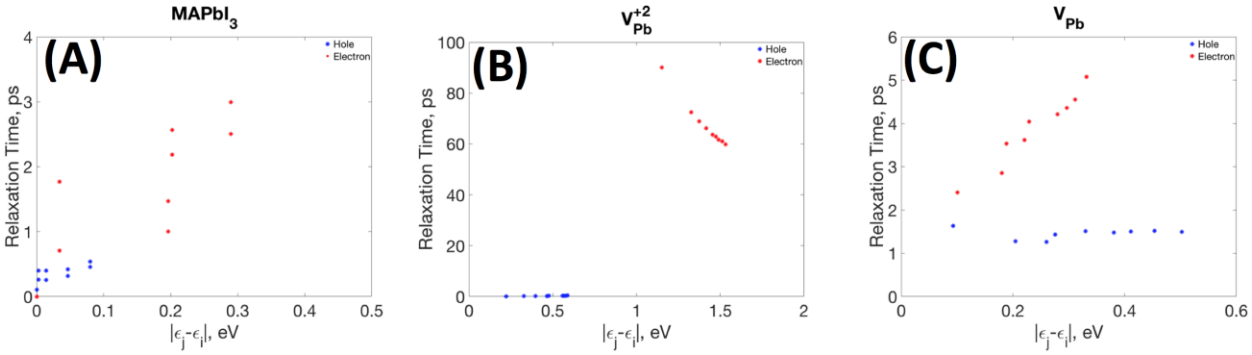

Figure S10. Closed shell non-radiative relaxation times for gamma point MD trajectories. The rates shown correspond to values found in **Table S2**.

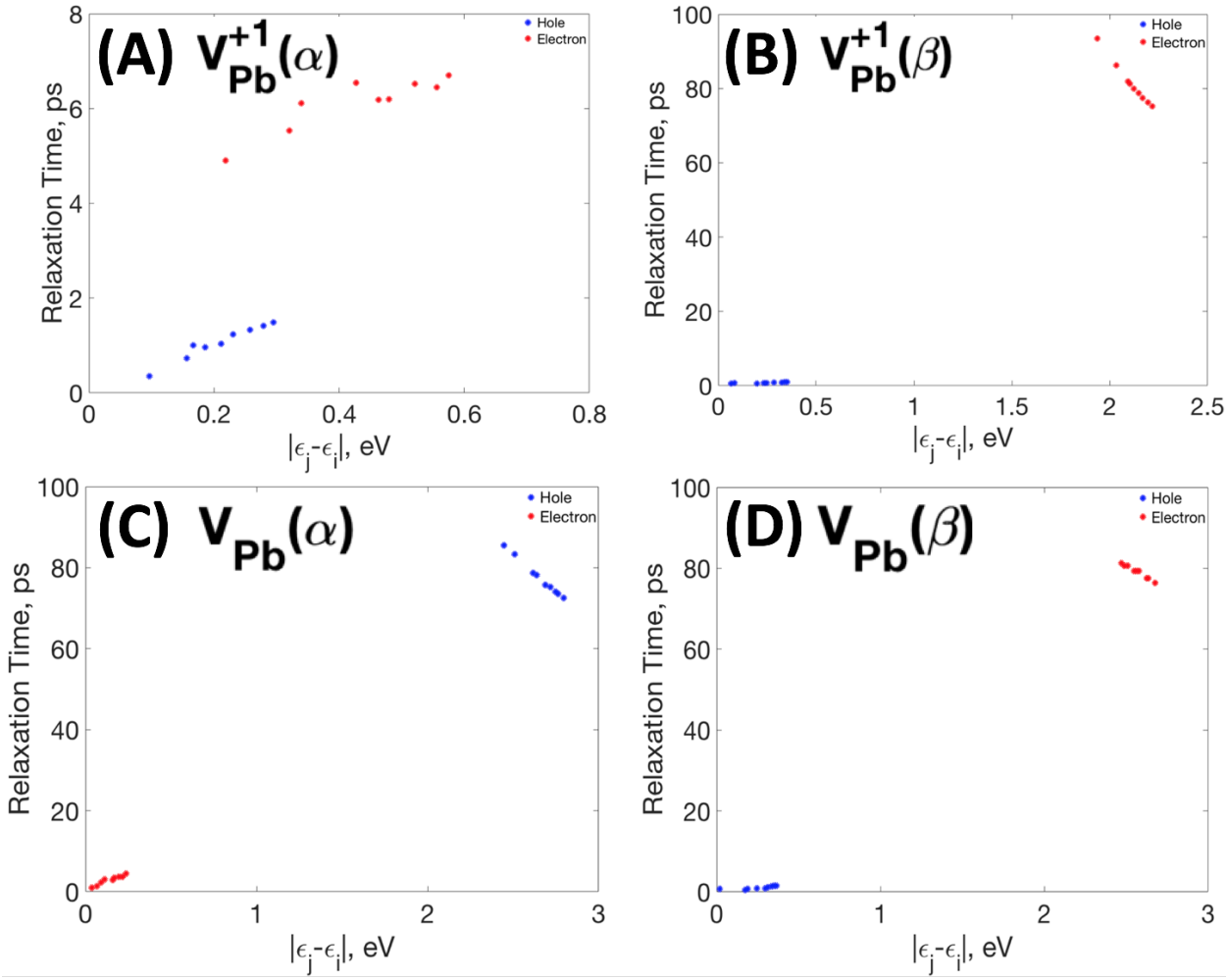

Figure S11. Open shell non-radiative relaxation times for gamma point MD trajectories. The rates shown correspond to values found in **Table S4**.

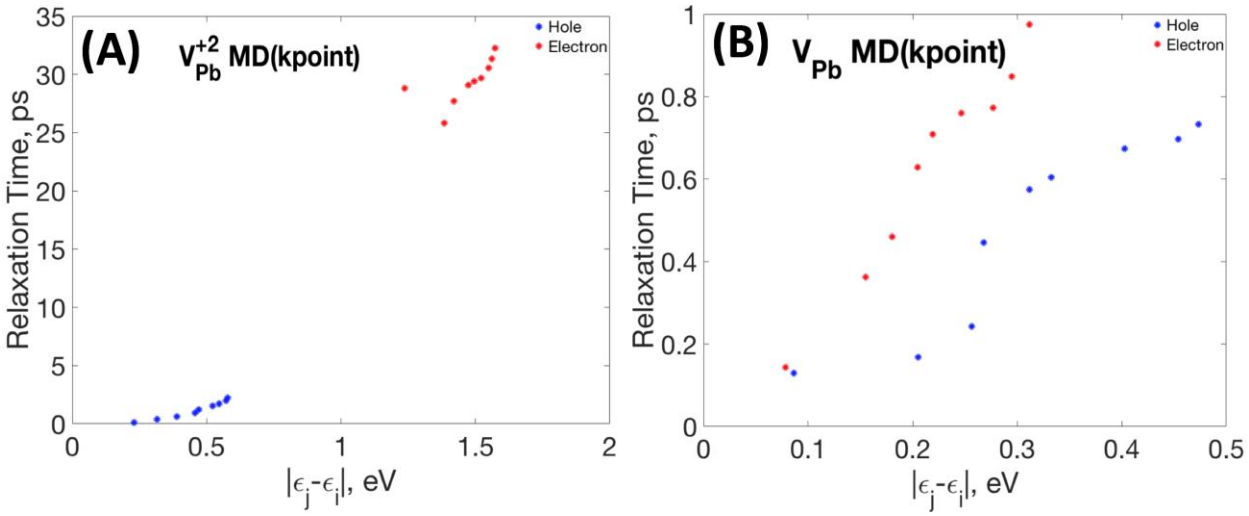

Figure S12. Closed shell non-radiative relaxation times for 2x2x2 k-point mesh MD trajectories. The rates shown correspond to values found in **Table S5**.

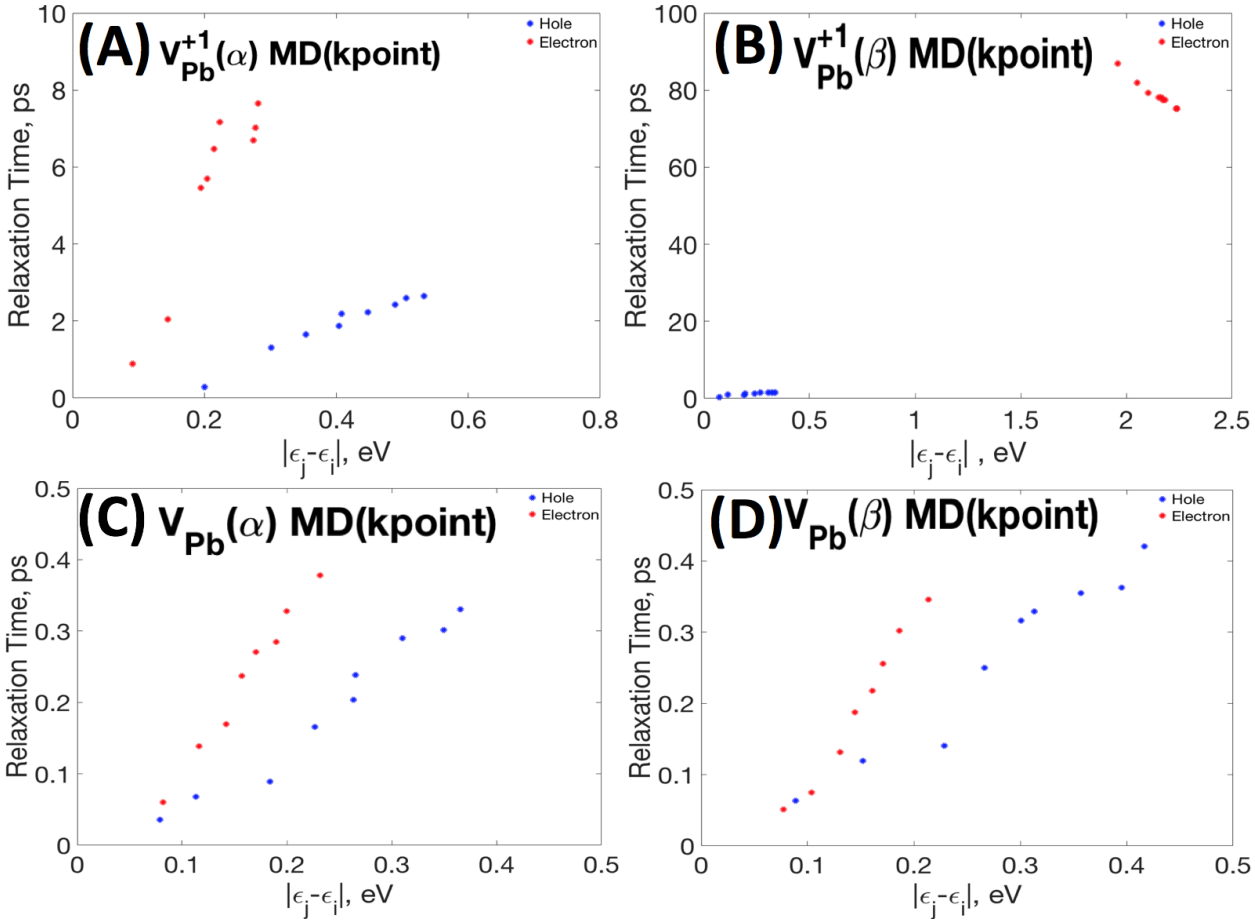

Figure S13. Open shell non-radiative relaxation times for 2x2x2 k-point mesh MD trajectories. The rates shown correspond to values found in **Table S5**.

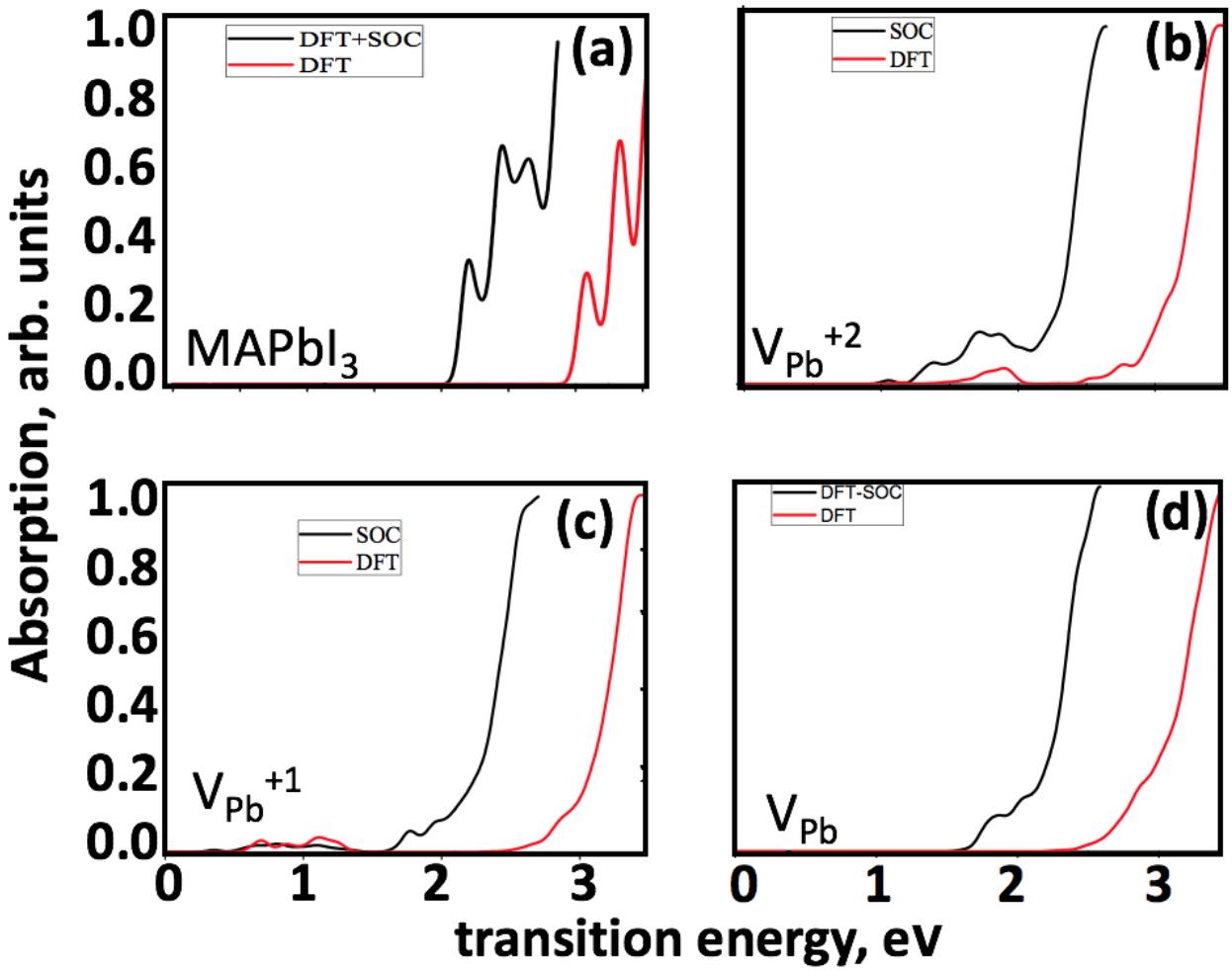

Figure S14. A comparison of DFT calculated absorption spectra with (black) and without (red) spin-orbit coupling for $MAPbI_3$ (a), V_{Pb}^{+2} (b), V_{Pb}^{+} (c), and V_{Pb} (d). The inclusion of spin-orbit coupling effects shows expected reduction of band gap energies in all systems under study.

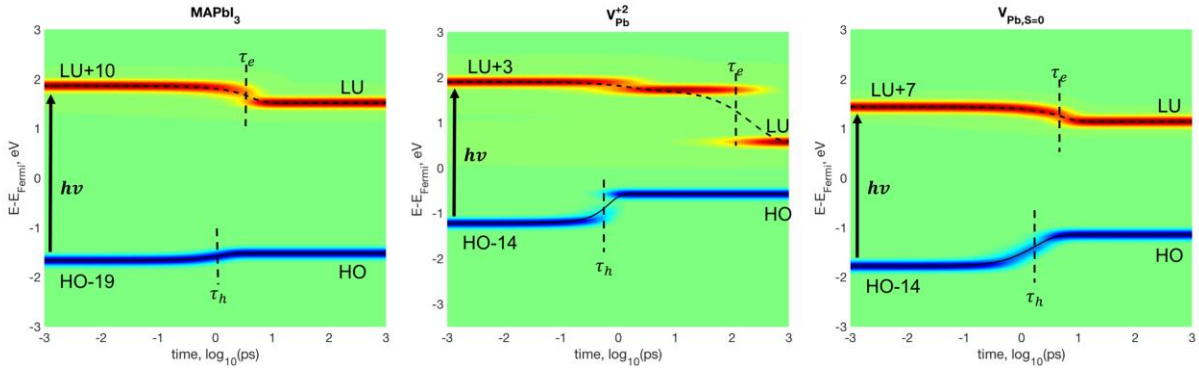

Figure S15. Visualization of a probable excitation, chosen via oscillator strength, and subsequent time dependent relaxation for the $MAPbI_3$ model. The image represents non-equilibrium electron density as a function of energy and time following photoexcitation with charges represented by no change(green), gain - electron(red), and loss - hole(blue). Each image shows initial electronic states of chosen transition, excitation (vertical arrow), lifetime of electron(τ_e) and hole (τ_h), and final LU and HO states. A high oscillator strength transition is shown for the closed shell models $MAPbI_3$ (left), V_{Pb}^{+2} (middle), and $V_{Pb,S=0}$ (right).

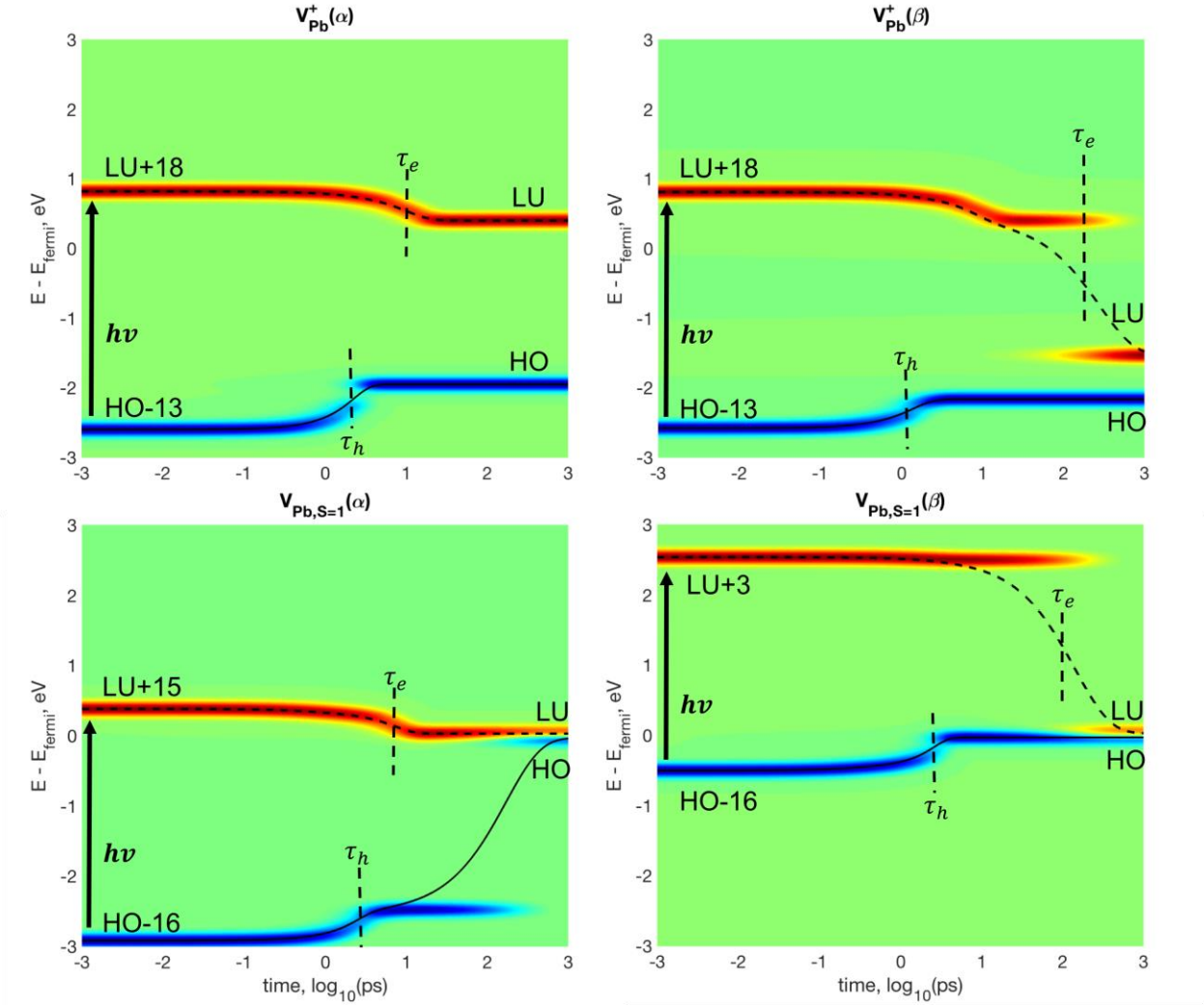

Figure S16. Visualization of a probable excitation, chosen via oscillator strength, and subsequent time dependent relaxation for the $MAPbI_3$ model. The image represents non-equilibrium electron density as a function of energy and time following photoexcitation with charges represented by no change(green), gain - electron(red), and loss - hole(blue). Each image shows initial electronic states of chosen transition, excitation (vertical arrow), lifetime of electron(τ_e) and hole (τ_h), and final LU and HO states. A high oscillator strength transition is shown for the charged (top) and triplet (bottom) α and β systems.

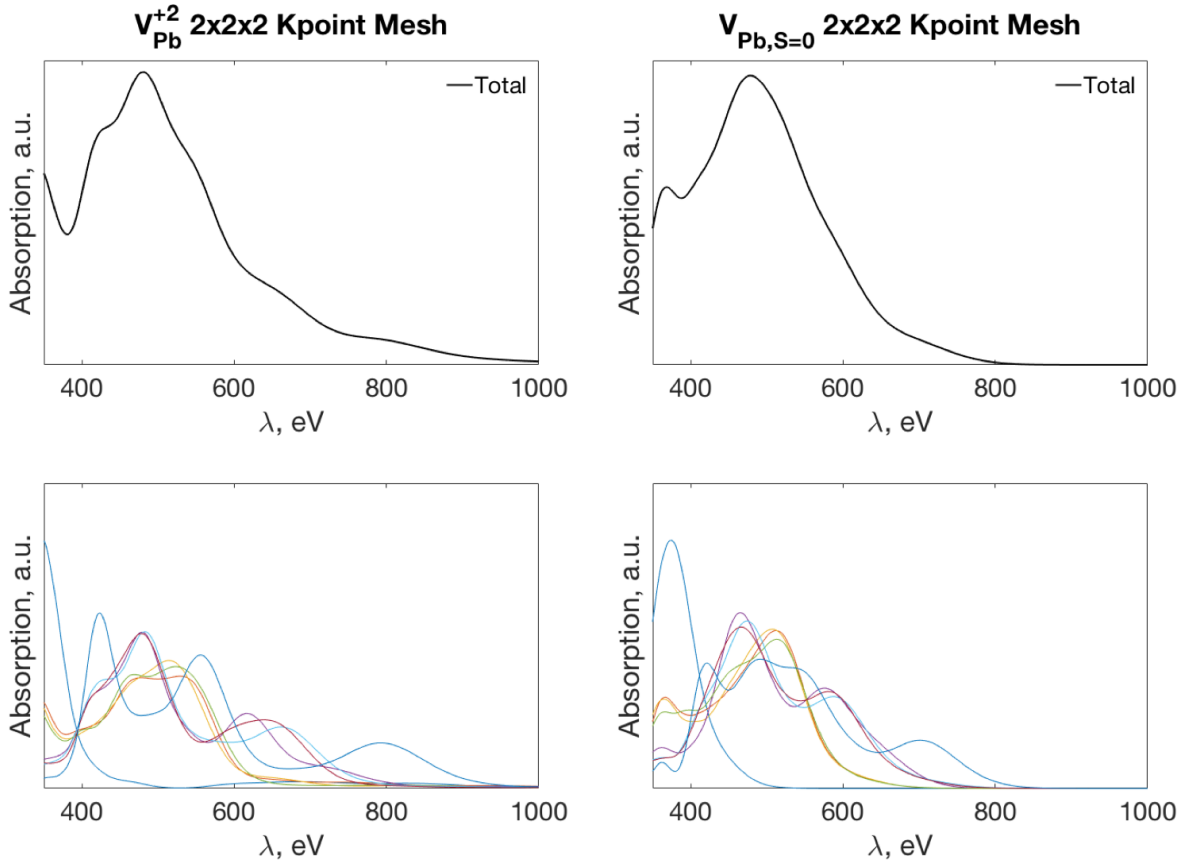

Figure S17. Absorption spectra computed with 2x2x2 k-point mesh. The total absorption (top) and partial absorption contributions by each k-point (bottom) are shown for the two closed shell vacancy systems, V_{Pb}^{+2} (left) and $V_{Pb,S=0}$ (right). Inclusion of all kpoints shows absorption onset previsouly missed by absorption spectra calculated at only the gamma point.

Table S1. The PBE total energies of five atomistic models considered in this work.

Model	$MAPbI_3$	V_{Pb}^{+2}	$V_{Pb(\sigma)}^{+}$	$V_{Pb,S=0}$	$V_{Pb,S=1}$
Total Energy (eV)	-1374.63	-1368.82	-1367.42	-1366.39	-1364.05

Table S2. The closed shell PBE total energies of a bulk lead material and the resulting energies from creating a vacancy in the Pb bulk and correcting the charge of the vacancy.

Model	Pb Bulk	Pb Bulk Vacancy	Pb Bulk Charge Corrected
Total Energy (eV)	-381.11	-377.87	-368.09

Table S3. Initial non-equilibrium electronic states and corresponding excitation energy, dE, oscillator strength, OS_STR, rate of hole, K_h, rate of electron, K_e, and lifetimes of the hole and electron.

$MAPbI_3$							
i	j	ΔE (eV)	OS_STR	k_h (ps^{-1})	k_e (ps^{-1})	τ_h (ps)	τ_e (ps)
656	686	3.5303	84.8171	1.0055	0.2909	0.99	3.43
657	687	3.5303	84.817	1.0647	0.2637	0.94	3.79
660	701	3.6906	60.4434	1.2717	0.1551	0.79	6.45
661	700	3.6906	60.4423	1.349	0.1591	0.74	6.29
666	681	3.3172	58.5346	1.867	0.6792	0.54	1.47
V_{Pb}^{+2}							
i	j	ΔE (eV)	OS_STR	k_h (ps^{-1})	k_e (ps^{-1})	τ_h (ps)	τ_e (ps)
542	524	3.1784	6.6778	0.3647	0.0213	2.75	46.95
550	519	3.4028	6.4504	0.1192	0.0269	8.39	37.17
562	508	3.6667	6.4107	0.1085	0.0285	9.22	35.09
551	518	3.4499	6.3502	0.1234	0.0261	8.1	38.31
554	525	3.4202	5.3167	0.117	0.0206	8.55	48.54
$V_{Pb(\alpha)}^{+}$							
i	j	ΔE (eV)	OS_STR	k_h (ps^{-1})	k_e (ps^{-1})	τ_h (ps)	τ_e (ps)
514	547	3.3881	6.5751	0.0396	0.1533	25.25	6.52
526	558	3.4215	6.4444	0.5441	0.1188	1.84	8.42
519	569	3.6597	6.0333	0.4602	0.03	2.17	33.33
506	553	3.5156	5.3399	0.2038	0.1246	4.91	8.03
503	567	3.7475	5.1798	0.1331	0.0822	7.51	12.16
$V_{Pb(\beta)}^{+}$							
i	j	ΔE (eV)	OS_STR	k_h (ps^{-1})	k_e (ps^{-1})	τ_h (ps)	τ_e (ps)
537	539	0.6966	9.4112	1.9016	NA	0.53	NA
536	539	0.7136	8.2172	1.3286	NA	0.75	NA
526	558	3.4192	7.4242	0.8085	0.0145	1.24	68.967
533	539	0.8768	7.3857	1.2999	NA	0.77	NA
519	569	3.6584	5.9037	0.6152	0.0169	1.63	59.17
$V_{Pb,S=0}$							
i	J	dE	OS_STR	Kh	Ke	Th	te
515	547	3.357	6.3499	.2626	.2296	3.81	4.36
504	548	3.461	5.5253	.0783	.2197	12.77	4.55
502	560	3.6469	5.2451	.1176	.1381	8.50	7.24
516	557	3.4926	5.241	.3193	.1511	3.13	6.62
502	564	3.7153	5.204	.1176	.0864	8.50	11.57
$V_{Pb,S=1,\alpha}$							
i	j	ΔE (eV)	OS_STR	k_h (ps^{-1})	k_e (ps^{-1})	τ_h (ps)	τ_e (ps)
540	541	0.2159	118.187	NA	NA	NA	NA
540	553	0.4324	49.837	NA	.1889	NA	5.29
540	542	0.26	37.602	NA	1.0895	NA	0.92
540	556	0.4605	35.656	NA	.1843	NA	5.43
540	549	0.3805	26.725	NA	.2752	NA	3.63
$V_{Pb,S=1,\beta}$							
i	j	ΔE (eV)	OS_STR	k_h (ps^{-1})	k_e (ps^{-1})	τ_h (ps)	τ_e (ps)
535	539	0.7991	6.3369	1.4529	NA	0.69	NA
531	539	0.9919	5.8382	.7734	NA	1.29	NA
534	539	0.8228	5.6821	1.2373	NA	0.81	NA
511	548	3.4566	4.3689	.1455	.0131	6.87	76.34
515	539	1.1057	4.3238	1.1678	NA	0.86	NA

Table S4. Non-radiative relaxation rates, $k_{e,h}$, and times, $\tau_{e,h}$, for gamma point MD trajectory. The values are for the perfect, $MAPbI_3$, neutral, V_{Pb}^{+2}, charged up, $V_{Pb}^{+1}(\alpha)$, charged down, $V_{Pb}^{+1}(\beta)$, singlet, V_{Pb}, triplet up, $V_{Pb}(\alpha)$, and triplet down, $V_{Pb}(\beta)$, systems. The value of iH&iE represent the number of states away from the band edges that are initially populated upon photoexcitation.

	iE/iH	ΔE_h (eV)	ΔE_e (eV)	k_e (ps^{-1})	k_h (ps^{-1})	τ_e (ps)	τ_h (ps)
$MAPbI_3$	2	0.000	0.000	0.000	9.42	0.000	0.106
	3	0.003	0.034	1.412	3.85	0.708	0.260
	4	0.003	0.034	0.565	2.52	1.770	0.398
	5	0.014	0.196	1.000	3.91	1.000	0.256
	6	0.014	0.196	0.679	2.50	1.472	0.400
	7	0.047	0.202	0.457	3.14	2.188	0.318
	8	0.047	0.202	0.389	2.38	2.569	0.420
	9	0.080	0.290	0.399	2.20	2.507	0.455
	10	0.080	0.290	0.334	1.87	2.992	0.536
V_{Pb}^{+2}	2	0.222	1.151	0.011	17.07	90.090	0.059
	3	0.328	1.326	0.014	7.58	72.464	0.132
	4	0.397	1.374	0.015	5.23	68.966	0.190
	5	0.465	1.415	0.015	4.60	66.225	0.217
	6	0.476	1.454	0.016	3.70	63.694	0.270
	7	0.558	1.475	0.016	3.42	62.893	0.293
	8	0.565	1.490	0.016	2.99	61.728	0.334
	9	0.577	1.511	0.016	2.70	60.976	0.371
	10	0.588	1.532	0.017	2.42	59.880	0.414
$V_{Pb(\alpha)}^{+}$	2	0.097	0.219	0.204	2.815	4.909	0.355
	3	0.156	0.320	0.181	1.365	5.531	0.733
	4	0.167	0.340	0.164	0.995	6.116	1.005
	5	0.186	0.427	0.153	1.039	6.545	0.963
	6	0.212	0.463	0.162	0.964	6.188	1.038
	7	0.230	0.479	0.162	0.813	6.192	1.230
	8	0.258	0.521	0.153	0.754	6.523	1.326
	9	0.279	0.556	0.155	0.710	6.452	1.409
	10	0.295	0.575	0.149	0.671	6.707	1.490
$V_{Pb(\beta)}^{+}$	2	0.067	1.935	0.011	1.902	93.458	0.526
	3	0.084	2.033	0.012	1.329	86.207	0.753
	4	0.197	2.093	0.012	1.792	81.967	0.558
	5	0.231	2.104	0.012	1.497	81.301	0.668
	6	0.247	2.122	0.013	1.300	80.000	0.769
	7	0.284	2.149	0.013	1.213	78.740	0.824
	8	0.323	2.168	0.013	1.155	77.519	0.866
	9	0.339	2.195	0.013	1.020	76.336	0.980
	10	0.353	2.217	0.013	0.962	75.188	1.040
$V_{Pb,S=0}$	2	0.093	0.101	0.416	0.614	2.404	1.630
	3	0.205	0.180	0.351	0.783	2.850	1.278
	4	0.260	0.189	0.283	0.792	3.530	1.263
	5	0.276	0.221	0.277	0.697	3.615	1.436
	6	0.330	0.229	0.247	0.661	4.045	1.512
	7	0.381	0.280	0.238	0.678	4.211	1.476
	8	0.411	0.296	0.230	0.666	4.355	1.502
	9	0.453	0.312	0.220	0.660	4.552	1.515
	10	0.502	0.332	0.197	0.669	5.074	1.495
$V_{Pb,S=1,\alpha}$	2	2.447	0.039	1.090	0.012	0.918	85.470
	3	2.508	0.068	0.731	0.012	1.367	83.333
	4	2.617	0.092	0.450	0.013	2.224	78.740
	5	2.638	0.112	0.328	0.013	3.051	78.125
	6	2.689	0.159	0.349	0.013	2.865	75.758
	7	2.719	0.169	0.298	0.013	3.361	75.188
	8	2.748	0.195	0.277	0.014	3.613	74.074
	9	2.762	0.216	0.275	0.014	3.634	73.529
	10	2.794	0.236	0.226	0.014	4.433	72.464
$V_{Pb,S=1,\beta}$	2	0.020	2.470	0.012	1.336	81.301	0.748
	3	0.174	2.487	0.012	2.442	80.645	0.410
	4	0.189	2.510	0.012	1.453	80.645	0.688
	5	0.246	2.548	0.013	1.237	79.365	0.808
	6	0.298	2.564	0.013	1.128	79.365	0.887
	7	0.312	2.577	0.013	0.900	79.365	1.111
	8	0.337	2.625	0.013	0.773	77.519	1.293
	9	0.349	2.635	0.013	0.697	77.519	1.436
	10	0.366	2.677	0.013	0.663	76.336	1.509

Table S5. Non-radiative relaxation rates, $k_{e,h}$, and times, $\tau_{e,h}$, for 2x2x2 k-point mesh MD trajectory. The values are for the perfect, $MAPbI_3$, neutral, V_{Pb}^{+2}, charged up, $V_{Pb}^{+1}(\alpha)$, charged down, $V_{Pb}^{+1}(\beta)$, singlet, V_{Pb}, triplet up, $V_{Pb}(\alpha)$, and triplet down, $V_{Pb}(\beta)$, systems. The value of iH&iE represent the number of states away from the band edges that are initially populated upon photoexcitation.

	iE/iH	ΔE_h (eV)	ΔE_e (eV)	k_e (ps^{-1})	k_h (ps^{-1})	τ_e (ps)	τ_h (ps)
V_{Pb}^{+2}	2	0.230	1.236	0.035	8.796	28.818	0.114
	3	0.315	1.385	0.039	2.604	25.840	0.384
	4	0.389	1.420	0.036	1.582	27.701	0.632
	5	0.457	1.474	0.034	1.084	29.070	0.922
	6	0.470	1.497	0.034	0.825	29.412	1.212
	7	0.523	1.522	0.034	0.650	29.674	1.539
	8	0.546	1.549	0.033	0.583	30.581	1.716
	9	0.572	1.561	0.032	0.500	31.348	2.001
	10	0.579	1.573	0.031	0.447	32.258	2.238

$V_{Pb(\alpha)}^{+}$	2	0.201	0.091	1.128	3.475	0.887	0.288	$V_{Pb(\beta)}^{+}$	2	0.074	1.958	0.012	3.323	86.957	0.301
	3	0.302	0.144	0.488	0.764	2.050	1.309		3	0.113	2.050	0.012	1.029	81.967	0.972
	4	0.354	0.195	0.183	0.608	5.461	1.645		4	0.190	2.104	0.013	1.089	79.365	0.918
	5	0.404	0.204	0.176	0.534	5.695	1.871		5	0.196	2.154	0.013	0.823	78.125	1.215
	6	0.408	0.215	0.155	0.457	6.468	2.186		6	0.241	2.165	0.013	0.765	78.125	1.308
	7	0.448	0.223	0.140	0.448	7.163	2.234		7	0.268	2.174	0.013	0.680	77.519	1.472
	8	0.490	0.275	0.150	0.412	6.689	2.427		8	0.304	2.184	0.013	0.689	77.519	1.452
	9	0.506	0.278	0.142	0.385	7.027	2.595		9	0.323	2.236	0.013	0.683	75.188	1.465
	10	0.533	0.282	0.131	0.377	7.651	2.653		10	0.338	2.239	0.013	0.651	75.188	1.536

$V_{Pb,S=0}$	2	0.086	0.079	6.975	7.701	0.143	0.130
	3	0.205	0.155	2.764	5.933	0.362	0.169
	4	0.257	0.180	2.175	4.119	0.460	0.243
	5	0.268	0.205	1.589	2.244	0.629	0.446
	6	0.312	0.219	1.411	1.741	0.709	0.575
	7	0.332	0.246	1.317	1.654	0.759	0.605
	8	0.403	0.277	1.294	1.483	0.773	0.674
	9	0.454	0.295	1.178	1.434	0.849	0.697
	10	0.473	0.312	1.026	1.363	0.975	0.733

$V_{Pb,S=1,\alpha}$	2	0.079	0.082	16.588	28.123	0.060	0.036	$V_{Pb,S=1,\beta}$	2	0.089	0.077	19.631	15.795	0.051	0.063
	3	0.113	0.116	7.218	14.788	0.139	0.068		3	0.152	0.104	13.350	8.375	0.075	0.119
	4	0.184	0.142	5.899	11.182	0.170	0.089		4	0.229	0.130	7.617	7.113	0.131	0.141
	5	0.226	0.157	4.212	6.034	0.237	0.166		5	0.267	0.145	5.323	3.995	0.188	0.250
	6	0.263	0.171	3.692	4.911	0.271	0.204		6	0.301	0.161	4.588	3.165	0.218	0.316
	7	0.266	0.190	3.514	4.192	0.285	0.239		7	0.313	0.171	3.906	3.039	0.256	0.329
	8	0.310	0.200	3.052	3.453	0.328	0.290		8	0.357	0.186	3.308	2.817	0.302	0.355
	9	0.349	0.232	2.645	3.316	0.378	0.302		9	0.395	0.214	2.889	2.756	0.346	0.363
	10	0.366	0.249	2.354	3.028	0.425	0.330		10	0.417	0.231	2.354	2.378	0.425	0.420

Table S6. Quantum yield values for all gamma point models under consideration.

Model	τ_{NR}	τ_R	ΔE	QY (%)
$MAPbI_3$	3.14E-06	6.6897	3.041	7.318
V_{Pb}^{+2}	2.14E-03	1.1076	1.1499	0.488
$V_{Pb(\alpha)}^{+}$	4.32E-06	0.768	2.3527	45.561
$V_{Pb(\beta)}^{+}$	5.25E-04	5.8226	0.63	1.250
$V_{Pb,S=0}$	1.74E-06	0.6971	2.2841	70.814
$V_{Pb,S=1,\alpha}$	4.05E-05	118.1875295	0.2159	6.434
$V_{Pb,S=1,\beta}$	4.87E-05	0.54144554	0.5836	63.098